JOC Article

Intramolecular Homolytic Translocation Chemistry: An ab Initio Study of 1,*n*-Silyl, Germyl, and Stannyl Group Transfer and Related Ring-Closure Reactions

Hiroshi Matsubara*,† and Carl H. Schiesser‡

Department of Chemistry, Faculty of Arts and Sciences, Osaka Prefecture University, Sakai, Osaka 599-8531, Japan, and School of Chemistry, Bio21 Molecular Science and Biotechnology Institute, The University of Melbourne, Victoria 3010, Australia

matsu@ms.cias.osakafu-u.ac.jp

Received July 17, 2003

Ab initio calculations using 6-311G**, cc-pVDZ, aug-cc-pVDZ, and a (valence) double-ζ pseudopotential (DZP) basis set, with (MP2, QCISD, CCSD(T)) and without (UHF) the inclusion of electron correlation, and density functional methods (B3LYP) predict that 1,*n*-homolytic transfers ($n = 1-5$) of silyl, germyl, and stannyl groups from group IV heteroatoms to carbon radicals can proceed via a frontside attack mechanism. At the B3LYP/DZP level of theory, energy barriers ($\Delta E^{\ddagger}$) of 101.2, 98.8, 58.9, and 63.4 kJ/mol are calculated for the 1,2-, 1,3-, 1,4-, and 1,5-translocation reactions, respectively, of SiH_3 between silicon atoms. Similar results are obtained for reactions involving germanium and tin with energy barriers ($\Delta E^{\ddagger}$) of 85.9−113.1, 84.4−109.0, 41.7−73.3, and 48.5−78.2 kJ/mol for the 1,2-, 1,3-, 1,4-, and 1,5-translocation reactions, respectively. This study also predicts that four- and five-membered ring-closure reactions can be competitive with the 1,4- and 1,5-translocation reactions. These results suggest that while 1,2- and 1,3-translocation four-membered ring-formation reactions are unlikely to be synthetically viable, 1,4- and 1,5-transfers and five-membered ring-formation have synthetic possibilities.

Introduction

Homolytic group or atom transfer (translocation) reactions, which often involve homolytic substitution by alkyl, aryl, and other radicals at heteroatoms such as silicon, germanium, tin, chalcogen, and halogen, are important free-radical processes[1] that can be useful in free-radical-based synthesis.[2] Radical Brook-type rearrangements,[3] the 1,3-stannyl shift reported by Tsuai and co-workers,[4] the 1,4-translocation of a cyano group shown by Cossy and co-workers,[5] and the 1,5- and 1,6-transfers of silyl, germyl, and stannyl groups reported by Kim and his associates[6] are representative of the direction that this chemistry is headed in (Scheme 1); other examples can be found in recent reviews.[7,8]

SCHEME 1

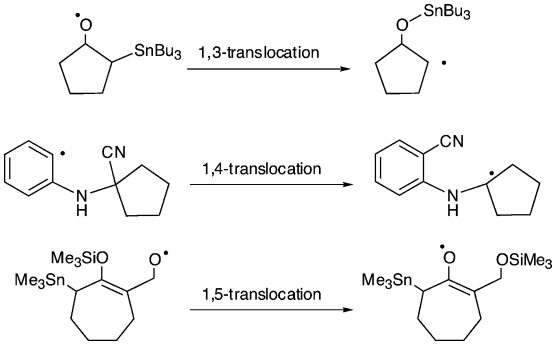

Work in our laboratories has been directed toward the design, application, and understanding of free-radical homolytic substitution chemistry with the aim of developing novel synthetic methodology.[9] To that end, we recently published several ab initio studies with the aim of increasing our understanding of the factors that affect and control the mechanism of homolytic substitution at

* Corresponding author. Phone: +81-72-254-9720. Fax: +81-72-254-9931.
† Osaka Prefecture University.
‡ The University of Melbourne.

(1) Schiesser, C. H.; Wild, L. M. *Tetrahedron* **1996**, *52*, 13256. Walton, J. C. *Acc. Chem. Res.* **1998**, *31*, 99. McCarroll, A. J.; Walton, J. C. *Angew. Chem., Int. Ed.* **2001**, *40*, 2224.

(2) Curran, D. P. *Synthesis* **1988**, 489. Curran, D. P. *Aldrichimica Acta* **2000**, *33*, 104.

(3) Dalton, J. C.; Bourque, R. A. *J. Am. Chem. Soc.* **1981**, *103*, 699. Tsai, Y.-M.; Cherng, C.-D. *Tetrahedron Lett.* **1991**, *32*, 3515.

(4) Chang, S.-Y.; Shao, Y.-F.; Chu, S.-F.; Fan, G.-T.; Tsai, Y.-M. *Org. Lett.* **1999**, *1*, 945.

(5) Cossy, J.; Poitevin, C.; Pardo, D. G.; Peglion, J. L. *Synthesis* **1995**, 1368.

(6) Kim, S.; Lee, S.; Koh, J. S. *J. Am. Chem. Soc.* **1991**, *113*, 5106. Kim, S.; Koh, J. S. *Chem. Commun.* **1992**, 1377. Kim, S.; Yeon, K. M.; Yoon, K. S. *Tetrahedron Lett.* **1997**, *38*, 3919. Kim, S.; Jung, M. S.; Cho, C. H.; Schiesser, C. H. *Tetrahedron Lett.* **2001**, *42*, 943. Kim, S.; Lim, K. M. *Chem. Commun.* **1993**, 1152.

(7) Robertson, J.; Pillai, J.; Lush, R. K. *Chem. Soc. Rev.* **2001**, *30*, 94. McCarrol, A. J.; Walton, C. W. *J. Chem. Soc., Perkin Trans. 1* **2001**, 3215. Studer, A.; Bossart, M. *Tetrahedron* **2001**, *57*, 9649.

(8) For some recent reports, see: Sano, H.; Asanuma, D.; Kosugi, M. *Chem. Commun.* **1999**, 1152. Amrein, S.; Bossart, M.; Vasella, T.; Studer, A. *J. Org. Chem.* **2000**, *65*, 4281. Allan, G. M.; Parson, A. F.; Pons, J.-F. *Synlett* **2002**, 1431. Sato, T.; Yamazaki, T.; Nakanishi, Y.; Uenishi, J.; Ikeda, M. *J. Chem. Soc., Perkin Trans. 1* **2002**, 1438. Sato, T.; Okamoto, K.; Nakano, Y.; Uenishi, J.; Ikeda, M. *Heterocycles* **2001**, *54*, 747.

10.1021/jo035037r CCC: $25.00
Published on Web 10/28/2003

several main-group higher heteroatoms. It is generally agreed that intramolecular homolytic substitution by a radical at a group (Y) proceeds via either a transition state (**1**) in which the attacking and leaving groups adopt a collinear (or nearly collinear) arrangement resulting in Walden inversion or with the involvement of a hypervalent intermediate (**2**) that may or may not undergo pseudorotation prior to dissociation.[10] We have also established that depending on the element undergoing translocation, a third *frontside* mechanism involving a transition state (**3**) is also possible. Roberts suggested that a similar mechanism might be important in hydrogen atom transfers between heteroatoms that have available orbitals and are not coordinately saturated.[11]

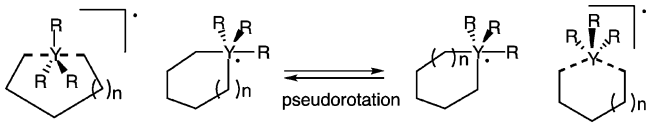

1 **2** **3**

Indeed, an extensive ab initio study of 1,2-translocations involving silicon-, germaniun-, and tin-containing groups predict that these reactions proceed via concerted mechanisms involving frontside homolytic substitution.[12,13] Similarly, intermolecular homolytic substitution involving silicon, germanium, and tin is predicted to proceed via both frontside and backside attack mechanisms.[14] As part of our ongoing interest in homolytic substitution chemistry involving main group higher heteroatoms, and in order to provide further insight into the mechanistic details of this chemistry, we began to explore 1,*n*-transfer reactions of silyl, germyl, and stannyl groups in *ω*-substituted radicals (**6**−**9**) (Scheme 2) using computational methods.

SCHEME 2

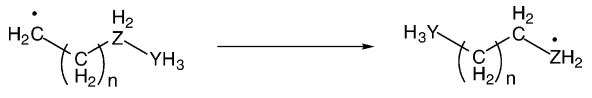

6: n = 0 **7**: n = 1 **8**: n = 2 **9**: n = 3

Y, Z = Si, Ge, Sn

10: n = 0 **11**: n = 1 **12**: n = 2 **13**: n = 3

During the course of these studies, our co-workers discovered an experimental example of a 1,4-migration reaction of a trimethylstannyl moiety from silicon to carbon; these studies revealed that the 1,4-shift of Me_3Sn can be competitive with ring-closure through intramolecular homolytic substitution of acyl radical at silicon with expulsion of Me_3Sn (Scheme 3).[15] Encouraged by these results, we also examined the analogous cyclization chemistry of the above-mentioned *ω*-substituted radicals. We report that 1,4- and 1,5-translocations are synthetically viable with B3LYP/DZP-calculated energy barriers of 36−73 kJ/mol, while 1,2- and 1,3-migrations are predicted not to be synthetically viable, with 80−104 kJ/mol energy barriers calculated at the same level of theory.

In competition, homolytic ring-closure reactions at silicon, germanium, and tin (Scheme 4) are found to involve both *backside* and *frontside* attack mechanisms, and five-membered ring-closure reactions are found to have similar activation energies to those of the competing 1,5-transfer reactions.

Methods

Ab initio and DFT molecular orbital calculations were carried out on Compaq Personal Workstation 600au and Alpha Station DS10L computers using the Gaussian 98 program.[16] Geometry optimizations were performed using standard gradient techniques at the SCF, MP2, and B3LYP levels of theory using restricted (RHF, RMP2, and RB3LYP) and unrestricted (UHF, UMP2, and UB3LYP) methods for closed- and open-shell systems, respectively.[17] All ground and transition states were verified by vibrational frequency analysis. Further single-point QCISD and CCSD(T) calculations were performed on each of the MP2 optimized structures, while for some 1,5-translocation reactions, QCISD and CCSD(T) single-point calculations were also performed on the B3LYP-optimized structures. When correlated methods were used, calculations were carried out using the frozen core approximation. Values of $\langle s^2 \rangle$ never exceeded 0.86 before annihilation of quartet contamination and were mostly 0.79 at correlated levels of theory. Where appropriate, zero-point vibrational energy (ZPE) corrections have been applied. Standard basis sets were used, as well as the (valence) double-ζ pseudopotential basis sets of Hay and Wadt[18] supplemented with a single set of *d*-type polarization functions for the heteroatoms in this study (exponents $d(\zeta)_{Si} = 0.284$,[19] $d(\zeta)_{Ge} = 0.230$,[19] and $d(\zeta)_{Sn} = 0.200$), together with the double-ζ all-electron basis sets of Dunning[20] with an additional set of polarization functions (exponents $d(\zeta)_C = 0.75$ (Y = Z = Si) and $p(\zeta)_H = 1.00$) for C

(9) Schiesser, C. H.; Sutej, K. *Tetrahedron Lett.* **1992**, *33*, 5137. Lyons, J. E.; Schiesser, C. H.; Sutej, K. *J. Org. Chem.* **1993**, *58*, 5632. Benjamin, L. J.; Schiesser, C. H.; Sutej, K. *Tetrahedron* **1993**, *49*, 2557. Fong, M. C.; Schiesser, C. H. *Tetrahedron Lett.* **1995**, *36*, 7329. Lucas, M. A.; Schiesser, C. H. *J. Org. Chem.* **1996**, *61*, 5754. Fong, M. C.; Schiesser, C. H. *J. Org. Chem.* **1997**, *62*, 3103. Laws, M. J.; Schiesser, C. H. *Tetrahedron Lett.* **1997**, *38*, 8429. Lucas, M. A.; Schiesser, C. H. *J. Org. Chem.* **1998**, *63*, 3032. Engman, L.; Laws, M. J.; Malmström, J.; Schiesser, C. H.; Zugaro, L. M. *J. Org. Chem.* **1999**, *64*, 6764. Lucas, M. A.; Nguyen, O. T. K.; Schiesser, C. H.; Zheng, S.-L. *Tetrahedron* **2000**, *56*, 3995. Al-Maharik, N.; Engman, L.; Malmström, J.; Schiesser, C. H. *J. Org. Chem.* **2001**, *66*, 6286. Kim, S.; Hovat, S. M.; Schiesser, C. H. *Aust. J. Chem.* **2002**, *55*, 753. Hovat, S. M.; Kim, S.; Schiesser, C. H. *Chem. Commun.* **2003**, 1182.

(10) Schiesser, C. H.; Wild, L. M. *Aust. J. Chem.* **1995**, *48*, 175. Howell, J. M.; Olsen, J. F. *J. Am. Chem. Soc.* **1976**, *98*, 7119. Cramer, C. J. *J. Am. Chem. Soc.* **1990**, *112*, 7965. Cramer, C. J. *J. Am. Chem. Soc.* **1991**, *113*, 2439.

(11) Roberts, B. P. *J. Chem. Soc., Perkin Trans. 2* **1996**, 2719.

(12) Hovat, S. M.; Schiesser, C. H. *J. Chem. Soc., Perkin Trans. 2* **2001**, 939.

(13) Schiesser, C. H.; Styles, M. L. *J. Chem. Soc., Perkin Trans. 2* **1997**, 2335.

(14) Matsubara, H.; Hovat, S. M.; Schiesser, C. H. *Org. Biomol. Chem.* **2003**, *1*, 1199.

(15) Studer, A.; Amrein, S.; Matsubara, H.; Schiesser, C. H.; Doi, T.; Kawamura, T.; Fukuyama, T.; Ryu, I. *Chem. Commun.* **2003**, 1190.

(16) Frisch, M. J.; Trucks, G. W.; Schlegel, H. B.; Scuseria, G. E.; Robb, M. A.; Cheeseman, J. R.; Zakrzewski, V. G.; Montgomery, J. A., Jr.; Stratmann, R. E.; Burant, J. C.; Dapprich, S.; Millam, J. M.; Daniels, A. D.; Kudin, K. N.; Strain, M. C.; Farkas, O.; Tomasi, J.; Barone, V.; Cossi, M.; Cammi, R.; Mennucci, B.; Pomelli, C.; Adamo, C.; Clifford, S.; Ochterski, J.; Petersson, G. A.; Ayala, P. Y.; Cui, Q.; Morokuma, K.; Malick, D. K.; Rabuck, A. D.; Raghavachari, K.; Foresman, J. B.; Cioslowski, J.; Ortiz, J. V.; Stefanov, B. B.; Liu, G.; Liashenko, A.; Piskorz, P.; Komaromi, I.; Gomperts, R.; Martin, R. L.; Fox, D. J.; Keith, T.; Al-Laham, M. A.; Peng, C. Y.; Nanayakkara, A.; Gonzalez, C.; Challacombe, M.; Gill, P. M. W.; Johnson, B. G.; Chen, W.; Wong, M. W.; Andres, J. L.; Head-Gordon, M.; Replogle, E. S.; Pople, J. A. *Gaussian 98*, revision A.7; Gaussian, Inc.: Pittsburgh, PA, 1998.

(17) Hehre, W. J.; Radom, L.; Schleyer, P. v. R.; Pople, P. A. *Ab Initio Molecular Orbital Theory*; Wiley: New York, 1986.

(18) Wadt, W. R.; Hay, P. J. *J. Chem. Phys.* **1985**, *82*, 284. Hay, P. J.; Wadt, W. R. *J. Chem. Phys.* **1985**, *82*, 270. Hay, P. J.; Wadt, W. R. *J. Chem. Phys.* **1985**, *82*, 299.

SCHEME 3

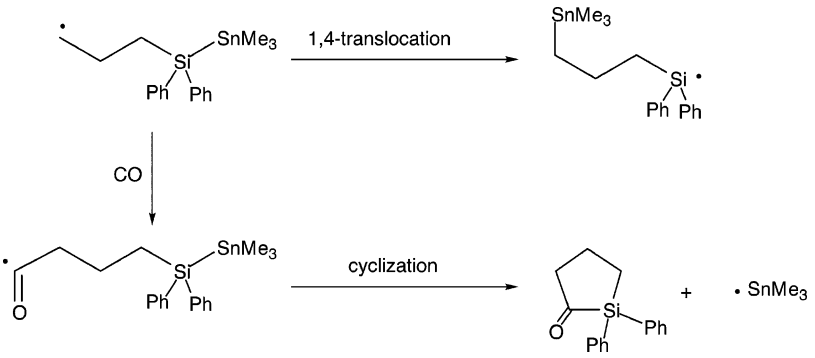

SCHEME 4

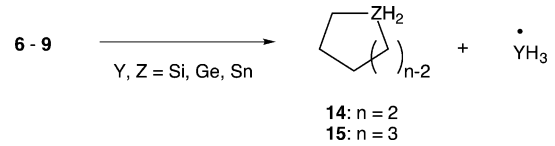

and H. We refer to this basis set as DZP throughout this work.[6,12,13,21−23] In previous work, results generated using DZP proved to be very similar to those obtained using 6-311G**.[12,13,22,23]

Optimized geometries and energies (Gaussian Archive Entries) for all structures in this study are available in Supporting Information.

Results and Discussion

1,2-Translocation Reactions in 6. Hypervalent species (**16**; Y, Z = Si, Ge, Sn) of C_1 symmetry were located on the $H_2CYH_2ZH_3$ (Y, Z = Si, Ge, Sn) potential energy surfaces at the UHF/DZP, MP2/DZP, and B3LYP/DZP levels of theory located. In addition, **16** (Y = Z = Si) was also optimized at the UHF/6-311G**, MP2/6-311G**, MP2/cc-pVDZ, MP2/aug-cc-pVDZ, and B3LYP/6-311G** levels of theory. Analysis of the force constants associated with structures **16** reveals that they correspond to the transition states for the rearrangement of radical **6** (Scheme 2).

Some typical transition structures **16** are summarized in Figure 1, while calculated energy barriers ($\Delta E_1^{\ddagger}$ and $\Delta E_2^{\ddagger}$, Scheme 6) and corresponding imaginary frequencies are listed in Table 1. The important geometric features of all structures **16** can be found in Figure S1 in Supporting Information. Figure 1 reveals that transition states **16** resemble those located for analogous intermolecular homolytic substitution reactions involving the frontside mechanism,[14] as well as those involved in other intramolecular homolytic 1,2-translocation reactions involving silicon, germanium, and tin.[12,13] Transition states **16** are predicted to involve attack angles (θ) in the range 41−49°; these angles are similar to those predicted for the transition states in other 1,2-translocation reactions involving silyl, germyl, and stannyl radicals,[12,13] and significantly more severe than those found for the analogous intermolecular reactions.[14,23] The size of the attack angle decreases in progressing from silicon to germanium and tin for the atom undergoing attack.

Inspection of Table 1 reveals that the calculated energy barriers ($\Delta E_1^{\ddagger}$) for the forward reaction (Scheme 6) are calculated to be smaller than those for the reverse reaction ($\Delta E_2^{\ddagger}$) at all levels of theory, indicating that these reactions are exothermic. The energy barrier ($\Delta E_1^{\ddagger}$) associated with transition state **16** (Y = Z = Si) is calculated to be 162.2 kJ/mol above the reactant carbon radical **6** using the UHF/6-311G** level of theory. As expected, electron correlation is important in these calculations; for example, MP2/6-311G** serves to lower this energy barrier to 101.9 kJ/mol. Interestingly, inclusion zero-point vibrational energy correction (ZPE) appears to have little effect on this number. Further improvements in basis set quality and correlation provide further reductions in $\Delta E_1^{\ddagger}$, which appears to converge to a value of about 100 kJ/mol. At the highest level of theory used (CCSD(T)/aug-cc-pVDZ//MP2/aug-cc-pVDZ), a $\Delta E_1^{\ddagger}$ value of 99.9 kJ/mol is predicted for reaction involving the 2,3-disilapropyl radical (**6**, Y = Z = Si). It is interesting to compare this value with that calculated using the B3LYP (density functional) method, which provides values of 97.3 kJ/mol (B3LYP/6-311G**) and 101.2 kJ/mol (B3LYP/DZP), while CCSD(T)/DZP//MP2/DZP provides a value some 10 kJ/mol higher. The data provided in Table 1 and in Table S2 (Supporting Infromation) reveal that the B3LYP/DZP level of theory predicts energy barriers that are comparable to those obtained at the CCSD(T)/aug-cc-pVDZ//MP2/aug-cc-pVDZ level, providing a useful benchmark and confidence in the performance of the B3LYP method in the systems in this study.

The values of $\Delta E_1^{\ddagger}$ appear to be principally dependent on the nature of the migrating group, while values of $\Delta E_2^{\ddagger}$ seem to be influenced by both the attacking and leaving

(19) Höllwarth, A.; Böhme, M.; Dapprich, S.; Ehlers, A. W.; Gobbi, A.; Jonas, V.; Köhler, K. F.; Stegmann, R.; Veldkamp, A.; Frenking, G. *Chem. Phys. Lett.* **1993**, *208*, 237.

(20) Dunning, T. H.; Hay, P. J. *Modern Theoretical Chemistry*; Plenum: New York, 1976; Chapter 1, pp 1−28.

(21) Lyons, J. E.; Schiesser, C. H. *J. Chem. Soc., Perkin Trans. 2* **1992**, 1655. Lyons, J. E.; Schiesser, C. H. *J. Organomet. Chem.* **1992**, *437*, 165. Smart, B. A.; Schiesser, C. H. *J. Chem. Soc., Perkin Trans. 2* **1994**, 2269. Schiesser, C. H.; Smart, B. A. *Tetrahedron* **1995**, *51*, 6051. Schiesser, C. H.; Smart, B. A.; Tran, T.-A. *Tetrahedron* **1995**, *51*, 10651. Schiesser, C. H.; Smart, B. A. *J. Comput. Chem.* **1995**, *16*, 1055. Schiesser, C. H.; Skidmore, M. A. *Chem. Commun.* **1996**, 1419. Schiesser, C. H.; Skidmore, M. A. *J. Organomet. Chem.* **1998**, *552*, 145. Schiesser, C. H.; Wild, L. M. *J. Org. Chem.* **1999**, *64*, 1131. Schiesser, C. H.; Smart, B. A.; Tran, T.-A. *Tetrahedron* **1995**, *51*, 3327.

(22) Schiesser, C. H.; Wild, L. M. *J. Org. Chem.* **1998**, *63*, 670. Schiesser, C. H.; Styles, M. L.; Wild, L. M. *J. Chem. Soc., Perkin Trans. 2* **1996**, 2257.

(23) Hovat, S. M.; Schiesser, C. H.; Wild, L. M. *Organometallics* **2000**, *19*, 1239.

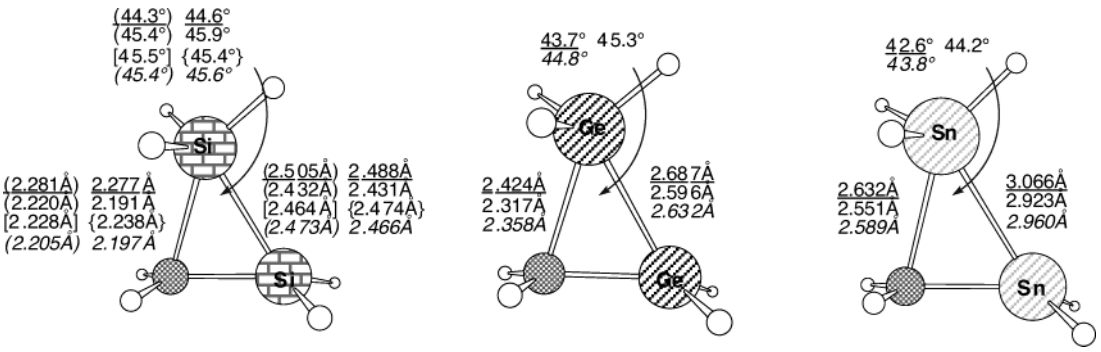

FIGURE 1. Optimized structure of typical transition states **16** for the rearrangement of radicals **6**. (UHF/6-311G**), UHF/DZP, (MP2/6-311G**), MP2/DZP, [MP2/cc-pVDZ], {MP2/aug-cc-pVDZ}, (*B3LYP/6-311G***), *B3LYP/DZP*.

SCHEME 5

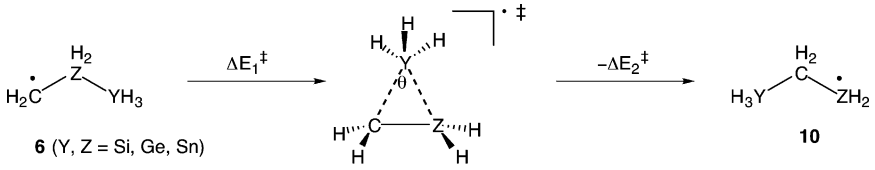

SCHEME 6

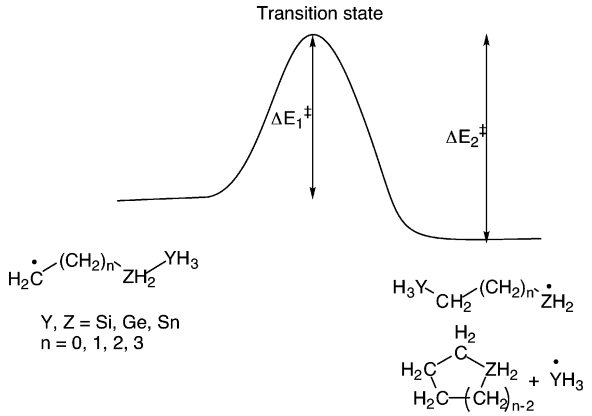

groups. As can be seen from the table, the reactivity for the 1,2-translocation reactions in this study is clearly Sn > Ge ∼ Si.

1,3-Translocation Reactions in 7. Intramolecular homolytic 1,3-migration of silyl, germyl, and stannyl groups from silicon, germanium, and tin to carbon atoms would involve the cyclic arrangement of atoms as depicted in Scheme 7. Within the geometric constraints imposed by this cyclic arrangement, there are two possible stereoisomeric transition states, **17** and **18**. Hypervalent species **17** of C_1 symmetry were located on the $H_2CCH_2YH_2ZH_3$ (Y, Z = Si, Ge, Sn) potential energy surfaces at the UHF/DZP, MP2/DZP, and B3LYP/DZP levels of theory.

In addition, **17** (Y = Z = Si) was also optimized at the UHF/6-311G**, MP2/6-311G**, MP2/cc-pVDZ, MP2/aug-cc-pVDZ, and B3LYP/6-311G** levels of theory. Analysis of the force constants associated with structures **17** (Y, Z = Si, Ge Sn) reveals that they correspond to the transition states for the rearrangement of radical **7** (Y, Z = Si, Ge, Sn). At all levels of theory employed, reactions involving transition states **17** were only found to involve the *frontside* mechanism, such that the attacking radical approaches from the same face as the leaving group. Interestingly, extensive searching of the potential energy surfaces failed to locate any intermediates or transition states **18** expected for *backside* attack at the hetroatoms in question. The typical transition structures **17** are summarized in Figure 2, while B3LYP/DZP-calculated energy barriers ($\Delta E_1^{\ddagger}$ and $\Delta E_2^{\ddagger}$, Scheme 6) and corresponding imaginary frequencies are listed in Table 2.

Inspection of Figure 2 reveals that MP2/DZP calculations predict the C−Y−Z transition state angles (θ) for these 1,3-translocations to be some 16−28° greater than those for the corresponding three-membered transition states located for the similar 1,2-migration reactions. It is also interesting to note that these angles (θ) are still about 16−28° smaller than those predicted for the analogous intermolecular homolytic substitution reactions involving the *frontside* attack mechanism. The smaller attack angles involved in the 1,3-transfers are likely to lead to considerable strain within these transition states. On the other hand, the C−Y and Y−Z distances in transition state **17** for the 1,3-translocation reactions are predicted to be shorter than those for the 1,2-migration reactions and longer than those for the similar intermolecular reactions.

Inspection of Tables 2 and S2 (Supporting Information) reveals that these reactions are predicted to be exothermic at most levels of theory. The energy barriers ($\Delta E_1^{\ddagger}$) associated with transition state **17** are calculated to be very similar to those for the 1,2-translocation reactions at the same level of theory, while ($\Delta E_2^{\ddagger}$) is predicted to be some 15−20 kJ/mol lower than those of the corresponding 1,2-translocation reactions. However, at the B3LYP/DZP level of theory, the values of $\Delta E_1^{\ddagger}$ and $\Delta E_2^{\ddagger}$ are still about 50 kJ/mol higher than those calculated for the analogous intermolecular homolytic substitution reactions.

1,4-Translocation Reactions in 8. Within the geometric constraints imposed by the cyclic arrangement depicted in Scheme 8 for intramolecular homolytic 1,4-

TABLE 1. Calculated Energy Barriers[a] ($\Delta E_1^{\ddagger}$ and $\Delta E_2^{\ddagger}$; Scheme 6) for the 1,2-Translocation Reactions of Radicals 6 and the Corresponding Imaginary Frequency[b] (ν)

Y	Z		$\Delta E_1^{\ddagger}$	$\Delta E_1^{\ddagger}$ + ZPE	$\Delta E_2^{\ddagger}$	$\Delta E_2^{\ddagger}$ + ZPE	ν
Si	Si	UHF/6-311G**	162.2	163.1	185.4	178.4	683.1i
		UHF/DZP	165.2	165.9	183.8	176.5	684.8i
		MP2/6-311G**	101.9	102.2	170.3	164.1	476.5i
		MP2/DZP	108.7	109.1	163.7	157.0	493.9i
		MP2/cc-pVDZ	102.4	102.6	165.2	158.6	486.1i
		MP2/aug-cc-pVDZ	96.6	96.6	159.8	153.6	470.9i
		QCISD/6-311G**//MP2/6-311G**	111.6		161.8		
		QCISD/DZP//MP2/DZP	117.6		155.3		
		QCISD/cc-pVDZ//MP2/cc-pVDZ	112.5		156.6		
		QCISD/aug-cc-pVDZ//MP2/aug-cc-pVDZ	107.5		151.9		
		CCSD(T)/6-311G**//MP2/6-311G**	104.6		157.8		
		CCSD(T)/DZP//MP2/DZP	111.2		151.3		
		CCSD(T)/cc-pVDZ//MP2/cc-pVDZ	105.7		152.5		
		CCSD(T)/aug-cc-pVDZ//MP2/aug-cc-pVDZ	99.9		147.3		
		B3LYP/6-311G**	97.3	96.7	138.8	131.4	442.2i
		B3LYP/DZP	101.2	100.5	139.0	131.6	458.5i
Si	Ge	UHF/DZP	166.7	167.7	207.5	199.3	667.2i
		MP2/DZP	109.8	111.0	190.1	183.4	521.4i
		QCISD/DZP//MP2/DZP	116.7		179.4		
		CCSD(T)/DZP//MP2/DZP	110.2		175.5		
		B3LYP/DZP	100.7	100.6	163.7	155.8	452.1i
Si	Sn	UHF/DZP	166.9	167.6	232.5	222.9	601.1i
		MP2/DZP	115.6	117.3	226.5	219.2	586.4i
		QCISD/DZP//MP2/DZP	118.5		210.1		
		CCSD(T)/DZP//MP2/DZP	111.6		206.4		
		B3LYP/DZP	101.7	102.2	193.2	184.8	462.6i
Ge	Si	UHF/DZP	163.5	163.6	162.6	155.2	626.3i
		MP2/DZP	112.2	112.1	151.1	144.6	522.9i
		QCISD/DZP//MP2/DZP	119.3		140.8		
		CCSD(T)/DZP//MP2/DZP	113.1		137.4		
		B3LYP/DZP	103.9	103.2	124.7	118.0	475.0i
Ge	Ge	UHF/DZP	163.5	163.9	181.8	173.6	585.3i
		MP2/DZP	112.3	113.1	173.8	167.3	518.1i
		QCISD/DZP//MP2/DZP	117.7		161.2		
		CCSD(T)/DZP//MP2/DZP	111.2		157.8		
		B3LYP/DZP	102.7	102.4	145.9	138.6	439.7i
Ge	Sn	UHF/DZP	162.0	162.2	200.1	190.7	503.1i
		MP2/DZP	116.9	118.2	204.4	197.5	560.4i
		QCISD/DZP//MP2/DZP	118.0		186.0		
		CCSD(T)/DZP//MP2/DZP	111.3		182.8		
		B3LYP/DZP	102.2	102.2	169.2	161.4	427.7i
Sn	Si	UHF/DZP	133.2	133.4	122.5	116.3	523.3i
		MP2/DZP	85.1	85.3	117.3	112.2	436.4i
		QCISD/DZP//MP2/DZP	91.8		105.6		
		CCSD(T)/DZP//MP2/DZP	86.3		103.0		
		B3LYP/DZP	78.8	78.2	92.8	87.2	381.0i
Sn	Ge	VHF/DZP	135.0	135.5	138.6	131.7	490.8i
		MP2/DZP	87.1	87.9	137.5	132.2	439.9i
		QCISD/DZP//MP2/DZP	91.6		123.2		
		CCSD(T)/DZP//MP2/DZP	85.9		120.7		
		B3LYP/DZP	78.7	78.4	110.6	104.4	349.8i
Sn	Sn	UHF/DZP	137.2	137.6	154.7	147.1	437.3i
		MP2/DZP	93.5	94.6	165.0	159.5	476.9i
		QCISD/DZP//MP2/DZP	93.8		144.9		
		CCSD(T)/DZP//MP2/DZP	87.9		142.7		
		B3LYP/DZP	80.2	80.3	131.3	125.2	345.6i

[a] Energies in kJ/mol. [b] Frequencies in cm^{-1}.

migrations of the type already discussed, there would appear to be two possible stereoisomeric transition states, **19** and **20**. Hypervalent species **19** of C_1 symmetry were located on the $H_2CCH_2CH_2YH_2ZH_3$ (Y, Z = Si, Ge, Sn) potential energy surfaces at the UHF/DZP, MP2/DZP, and B3LYP/DZP levels of theory. Analysis of the force constants associated with structures **19** (Y, Z = Si, Ge, Sn) reveals that these structures are the transition states for the rearrangement of radical **8** (Y, Z = Si, Ge, Sn).

At all levels of theory employed, reactions involving transition states **19** were all found to involve the *frontside* mechanism; no intermediates or transition states **20** for the *backside* attack were able to be located. Typical transition structures **19** are summarized in Figure 3, while B3LYP/DZP-calculated energy barriers ($\Delta E_1^{\ddagger}$ and $\Delta E_2^{\ddagger}$, Scheme 6) and corresponding imaginary frequencies are listed in Table 3 (important geometric features of all transition structures in this study can be found in Figures S1−S9 in Supporting Information, while calculated energy barriers at all levels of theory employed in this study are listed in Tables S1−S7 in Supporting Information). As can be seen in Figure 3, transition states

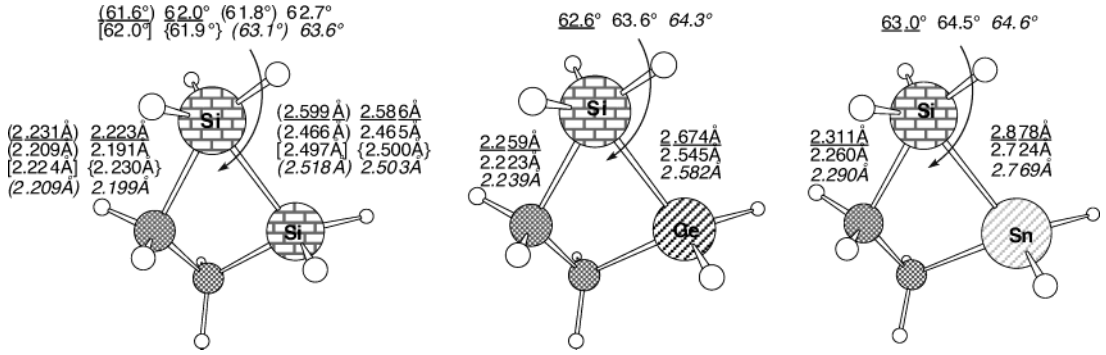

FIGURE 2. Optimized structure of typical transition state **17** for the rearrangement of radicals **7**. (UHF/6-311G**), UHF/DZP, (MP2/6-311G**), MP2/DZP, [MP2/cc-pVDZ], {MP2/aug-cc-pVDZ}, (*B3LYP/6-311G***), *B3LYP/DZP*.

SCHEME 7

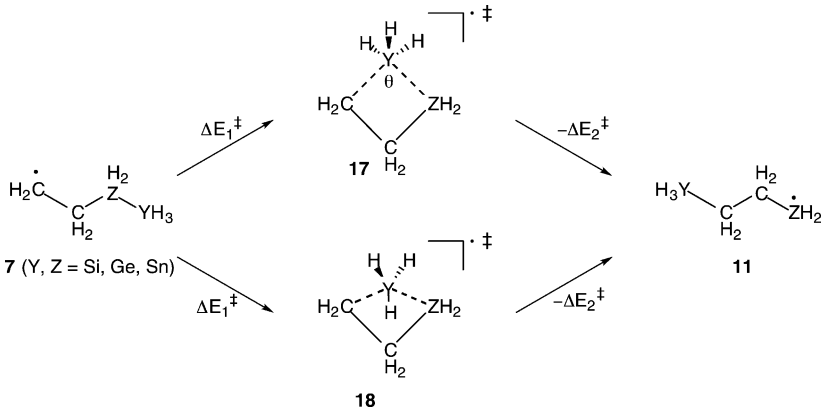

TABLE 2. B3LYP/DZP-Calculated Energy Barriers[a] ($\Delta E_1^{\ddagger}$ and $\Delta E_2^{\ddagger}$; Scheme 6) for the 1,3-Translocation Reactions of Radicals 7 and the Corresponding Imaginary Frequency[b] (ν)

Y	Z	$\Delta E_1^{\ddagger}$	$\Delta E_1^{\ddagger}$ + ZPE	$\Delta E_2^{\ddagger}$	$\Delta E_2^{\ddagger}$ + ZPE	ν
Si	Si	98.8	100.7	118.7	113.2	401.5i
Si	Ge	96.7	98.2	133.3	126.8	404.6i
Si	Sn	94.1	95.9	150.2	143.3	412.2i
Ge	Si	101.7	103.4	105.5	100.1	374.4i
Ge	Ge	98.7	100.2	116.8	111.0	360.6i
Ge	Sn	96.4	97.9	130.1	123.5	365.2i
Sn	Si	80.4	82.0	73.5	69.2	313.9i
Sn	Ge	79.8	81.0	82.8	78.0	299.7i
Sn	Sn	80.6	81.9	94.3	88.8	305.5i

[a] Energies in kJ/mol. [b] Frequencies in cm^{-1}.

TABLE 3. B3LYP/DZP-Calculated Energy Barriers[a] ($\Delta E_1^{\ddagger}$ and $\Delta E_2^{\ddagger}$; Scheme 6) for the 1,4-Translocation Reactions of Radicals 8 and the Corresponding Imaginary Frequency[b] (ν)

Y	Z	$\Delta E_1^{\ddagger}$	$\Delta E_1^{\ddagger}$ + ZPE	$\Delta E_2^{\ddagger}$	$\Delta E_2^{\ddagger}$ + ZPE	ν
Si	Si	58.9	62.4	91.1	86.1	238.5i
Si	Ge	52.9	56.9	105.1	99.8	284.3i
Si	Sn	47.4	51.9	125.3	119.7	299.3i
Ge	Si	66.0	69.0	82.0	77.3	238.8i
Ge	Ge	58.6	62.1	92.3	87.4	229.9i
Ge	Sn	52.7	56.6	108.0	102.8	239.2i
Sn	Si	46.0	49.6	51.5	48.3	215.8i
Sn	Ge	40.4	43.9	59.1	55.3	195.0i
Sn	Sn	36.0	40.1	71.4	67.6	190.4i

[a] Energies in kJ/mol. [b] Frequencies in cm^{-1}.

19 involved in the 1,4-translocation reactions of silyl, germyl, and stannyl groups are predicted to adopt the half-chair conformation at all of levels of theory employed. As expected, the C−Y−Z transition state angles (θ) for these 1,4-translocation reactions are predicted to be greater than those for the corresponding 1,2- and 1,3-processes and almost the same as those predicted for the analogous intermolecular *frontside* homolytic substitution reactions, indicating that there is minimal strain in transition states **19** for these 1,4-migration reactions. The C−Y and Y−Z distances in transition states **19** are shorter than those in transition states **16** and **17** for the 1,2- and 1,3-translocation reactions, respectively, and similar to the separations of the *frontside* transition states for intermolecular substitution reactions. These observations are, once again, indicative of the differing levels of strain in the various cyclic transition structures involved in the chemistry under consideration.

Inspection of Table 3 reveals some interesting trends in energy. It is clear from Table 3 that these reactions are all predicted to be exothermic at the B3LYP/DZP level of theory. As observed in previous work, for given attacking and leaving radicals involved at the group IV heteroatom, the order of reactivity is usually Sn > Si ≥ Ge.[23] The results reported here reveal the same trend, namely, that the order of reactivity for 1,4-migration of a group IV heteroatom from the same group is: Sn > Si > Ge. On the other hand, the order of reactivity for 1,4-migration of a group from the same group IV heteroatom is Sn > Ge > Si. It is instructive to compare these results with those determined recently by our colleagues. For the 1,4-translocation depicted in Scheme 3, preliminary experiments provided values for the energy barrier of 46

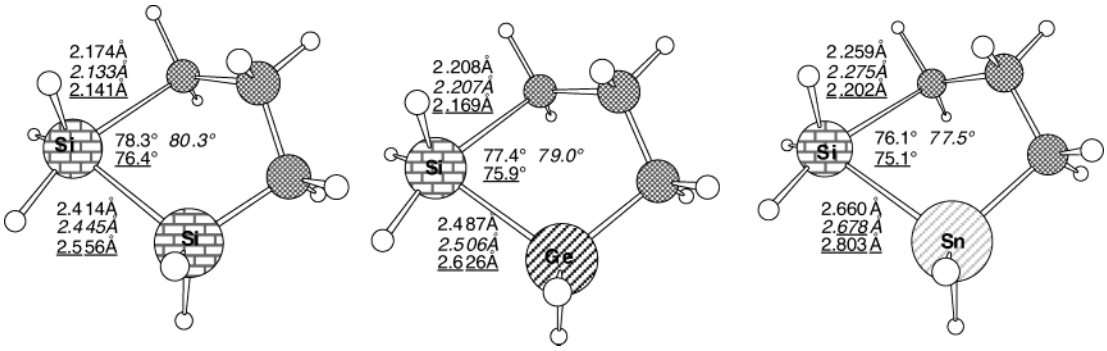

FIGURE 3. MP2/DZP-optimized structure of typical transition state **19** for the rearrangement of radicals **8**. B3LYP/DZP values are in italics, UHF/DZP values are underlined.

SCHEME 8

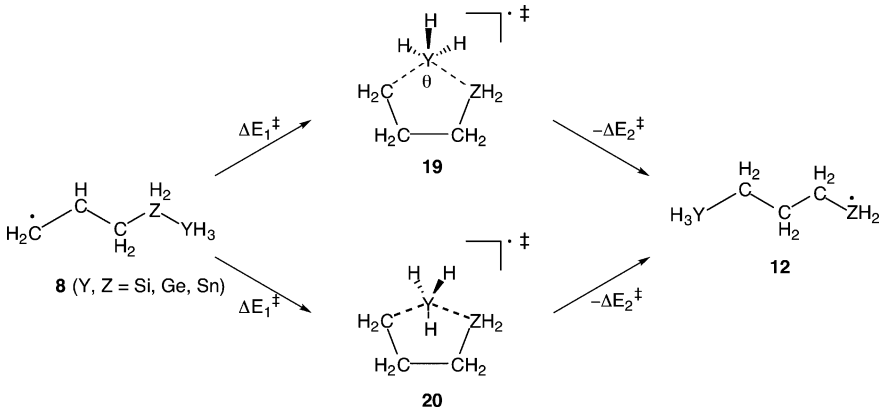

TABLE 4. B3LYP/DZP-Calculated Energy Barriers[a] ($\Delta E_1^{\ddagger}$ and $\Delta E_2^{\ddagger}$; Scheme 6) for the 1,5-Translocation Reactions of Radicals 9 and the Corresponding Imaginary Frequency[b] (ν) of Transition State 21

Y	Z	$\Delta E_1^{\ddagger}$	$\Delta E_1^{\ddagger}$ + ZPE	$\Delta E_2^{\ddagger}$	$\Delta E_2^{\ddagger}$ + ZPE	ν
Si	Si	63.4	68.4	95.4	91.5	197.5i
Si	Ge	58.0	63.5	110.1	106.6	261.3i
Si	Sn	53.1	59.4	131.3	127.4	288.8i
Ge	Si	72.5	76.6	88.3	84.5	241.1i
Ge	Ge	65.9	70.2	99.5	95.3	216.4i
Ge	Sn	60.2	65.7	115.8	111.7	219.1i
Sn	Si	53.4	57.8	58.5	56.3	220.9i
Sn	Ge	48.7	53.4	67.0	64.3	190.5i
Sn	Sn	45.5	50.3	80.8	77.8	167.6i

[a] Energies in kJ/mol. [b] Frequencies in cm^{-1}.

TABLE 5. Calculated Energy Barriers[a] ($\Delta E_1^{\ddagger}$ and $\Delta E_2^{\ddagger}$; Scheme 6) for the 1,5-Translocation Reactions of Radicals 9 and the Corresponding Imaginary Frequency[b] (ν) of Transition State 22

Y	Z		$\Delta E_1^{\ddagger}$	$\Delta E_1^{\ddagger}$ + ZPE	$\Delta E_2^{\ddagger}$	$\Delta E_2^{\ddagger}$ + ZPE	ν
Ge	Si	B3LYP/DZP	74.6	79.5	90.4	87.4	251.6i
Sn	Si	B3LYP/DZP	55.5	60.6	60.6	59.1	233.1i
Sn	Ge	UHF/DZP	123.2	129.7	113.4	111.2	425.5i
Sn	Sn	UHF/DZP	119.1	125.7	122.3	119.4	407.7i

[a] Energies in kJ/mol. [b] Frequencies in cm^{-1}.

kJ/mol,[15] which is in excellent agreement with our calculations on the reaction involving the similar radical **8** (Y = Sn, Z = Si), where $\Delta E_1^{\ddagger}$ + ZPE is predicted to be 49.6 kJ/mol at the B3LYP/DZP level of theory.

It is also interesting to note that the energy barriers ($\Delta E_1^{\ddagger}$) for 1,4-translocation reaction involving **19** are calculated to be very similar to those determined for the intermolecular substitution chemistry involving the *frontside* attack mechanism,[14] further evidence that transition states **19** are essentially strain-free.

1,5-Translocation Reactions in 9. In a fashion similar to the 1,4-translocations discussed above, we were able to locate hypervalent species **21** and **22** as transition states for the rearrangement of radical **9** (Y, Z = Si, Ge, Sn) (Scheme 9). Clearly, structures **21** and **22** are stereoisomeric structures involved in the *frontside* mechanism. Additionally, extensive searching of the various potential energy surfaces failed to locate any intermediates or transition states **23** for the *backside* attack at the hetroatoms in each case.

The important geometrical features of typical structures **21** and **22** are summarized in Figures 4 and 5, while B3LYP/DZP calculated energy barriers ($\Delta E_1^{\ddagger}$ and $\Delta E_2^{\ddagger}$, Scheme 6) and the corresponding transition state imaginary frequencies are listed in Tables 4 and 5.

Inspection of Figures 4 and 5 reveals that transition states **21** and **22** are both predicted to adopt chairlike conformations. These two structures differ only in the orientation of the hydrogen atoms on the migrating group, with **21** containing an axially disposed hydrogen atom, while the similar hydrogen atom in **22** is equatorial. It is interesting to note that while transition states **21** were located for all systems at all levels of theory in this study, transition states **22** were only located for the cases displayed in Figure 5 at the UHF/DZP and B3LYP/DZP levels of theory.

The C−Y−Z transition state attack angles (θ) for the 1,5-translocation reactions are predicted to be very

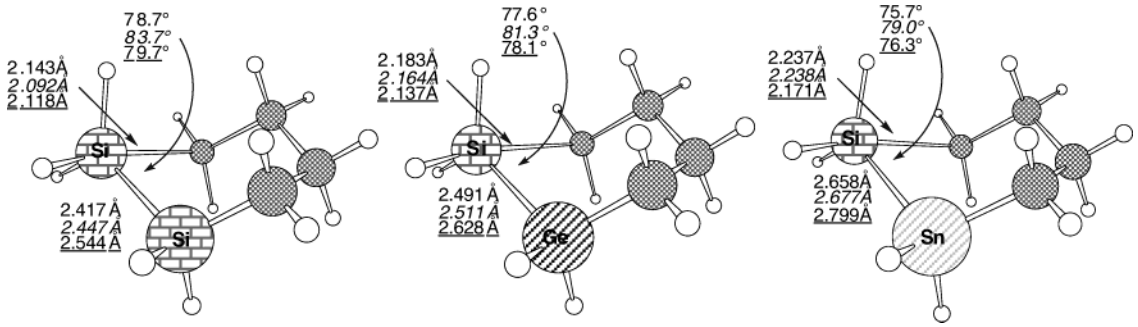

FIGURE 4. MP2/DZP-optimized structure of typical transition state **21** for the rearrangement of radicals **9**. B3LYP/DZP values are in italics. UHF/DZP values are underlined.

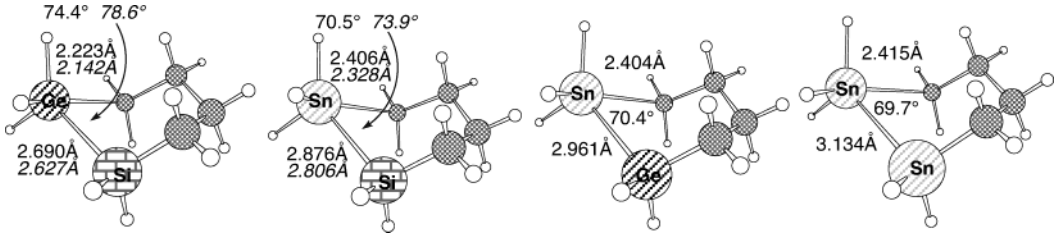

FIGURE 5. UHF/DZP-optimized structure of transition state **22** for the rearrangement of radicals **9**. B3LYP/DZP values are in italics.

SCHEME 9

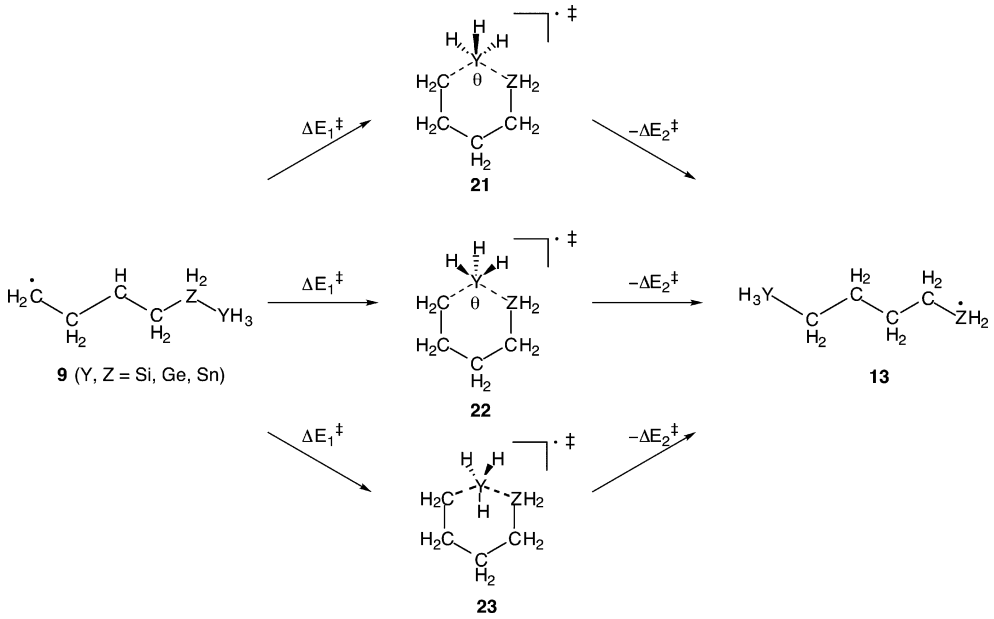

similar to those for the 1,4-migration reactions, indicating that there is also little strain in transition states **21** involved in 1,5-migration reactions. In addition, the C−Y and Y−Z distances in transition states **21** are very close to those of transition states **12** for 1,4-translocation reactions. Interestingly, the C−Y−Z transition state attack angles (θ) in transition states **22** are predicted to be slightly smaller (up to 3°) than those in transition states **21**, while C−Y and Y−Z distances in the transition states **22** are predicted to be close to those of transition states **21**.

Tables 4 and 5, and S4 and S5 in Supporting Information, reveal that these reactions are predicted to be exothermic at all levels of theory that incorporate electron correlation. The energy barriers ($\Delta E_1^{\ddagger}$) for 1,5-translocation reaction involving **21** are calculated to be only very slightly larger than those for the analogous 1,4-translocation reactions discussed above, suggesting that both *frontside* pathways are feasible. The predicted order of reactivity reveals the same trends as for the 1,4-translocation reactions presented earlier.

Competitive Ring-Closure Reactions: Formation of Four-Membered Rings. Extensive search of the $H_2CCH_2CH_2YH_2ZH_3$ (Y, Z = Si, Ge, Sn) potential energy surfaces at the UHF/DZP, MP2/DZP, and B3LYP/DZP levels of theory located structures **24** and **25** as transition states for the ring-closure of radical **8** (Y, Z = Si, Ge, Sn), resulting in the formation of the metallacyclobutane (**14**) and the expulsion of a group IV heteroatom-centered radical (Scheme 10). Force−constant analysis confirmed

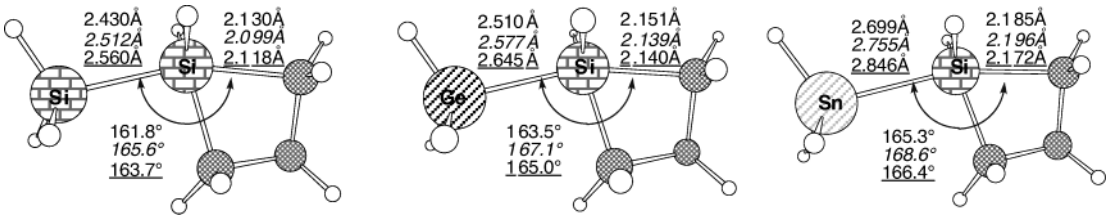

FIGURE 6. MP2/DZP-optimized structure of typical transition state **24** for the *backside* attack mechanism of ring-closure reactions of radicals **8**. B3LYP/DZP values are in italics. UHF/DZP values are underlined.

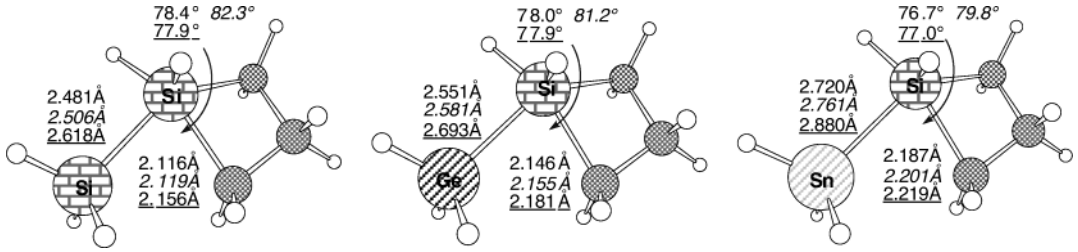

FIGURE 7. MP2/DZP-optimized structure of typical transition state **25** for the *frontside* attack mechanism of ring-closure reactions of radicals **8**. B3LYP/DZP values are in italics. UHF/DZP values are underlined.

SCHEME 10

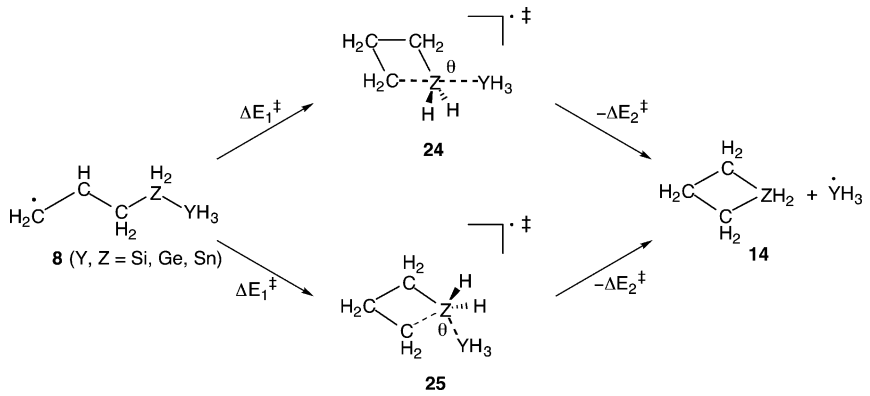

TABLE 6. B3LYP/DZP-Calculated Energy Barriers[a] ($\Delta E_1^{\ddagger}$ and $\Delta E_2^{\ddagger}$; Scheme 6) for the Four-Membered Ring-Closure Reactions of Radicals 8 and the Corresponding Imaginary Frequency[b] (ν) of Transition State 24 and 25

		24					25				
Y	Z	$\Delta E_1^{\ddagger}$	$\Delta E_1^{\ddagger}$ + ZPE	$\Delta E_2^{\ddagger}$	$\Delta E_2^{\ddagger}$ + ZPE	ν	$\Delta E_1^{\ddagger}$	$\Delta E_1^{\ddagger}$ + ZPE	$\Delta E_2^{\ddagger}$	$\Delta E_2^{\ddagger}$ + ZPE	ν
Si	Si	96.3	96.3	35.7	37.2	462.0i	98.3	99.9	37.7	40.7	280.0i
Si	Ge	c					100.0	100.6	24.6	26.9	205.2i
Si	Sn	c					c				
Ge	Si	86.8	86.8	45.9	46.3	507.5i	89.1	90.7	48.1	50.3	298.1i
Ge	Ge	89.8	89.7	31.9	32.4	354.8i	91.0	91.8	33.1	34.5	245.6i
Ge	Sn	c					c				
Sn	Si	76.4	76.6	62.9	62.0	542.8i	76.8	78.7	63.3	64.1	323.6i
Sn	Ge	79.2	78.7	44.8	44.2	411.9i	79.7	80.5	45.3	46.0	276.8i
Sn	Sn	c					63.3	64.8	12.9	13.8	150.7i

[a] Energies in kJ/mol. [b] Frequencies in cm^{-1}. [c] No transition states were found.

that structures **24** and **25** correspond to the transition states for the *backside* and *frontside* mechanisms, respectively; typical structures are displayed in Figures 6 and 7, respectively,† while B3LYP/DZP-calculated energy barriers ($\Delta E_1^{\ddagger}$ and $\Delta E_2^{\ddagger}$, Scheme 6) and corresponding imaginary frequencies are listed in Table 6. It should be noted that we were unable to locate either a transition state or an intermediate in some cases.

The *backside* structure **24**, is predicted to adopt an arrangement of attacking and leaving groups ($\theta = 157-169°$) that appreciably deviate from the ideal collinear arrangement. In the case of the *frontside* structures **25**, these are predicted to have attack angles (θ) of about 71−82°, very similar to those predicted for the analogous intermolecular reaction involving group IV heteroatoms.[14] Inspection of Table 6 reveals that, unlike the translocation reaction discussed above, these cyclization reactions are predicted to be endothermic, presumably due to the strain involved in forming the four-membered metallocycles. However, the reactivity trends observed are the same as those predicted for the 1,4-translocation chemistry.

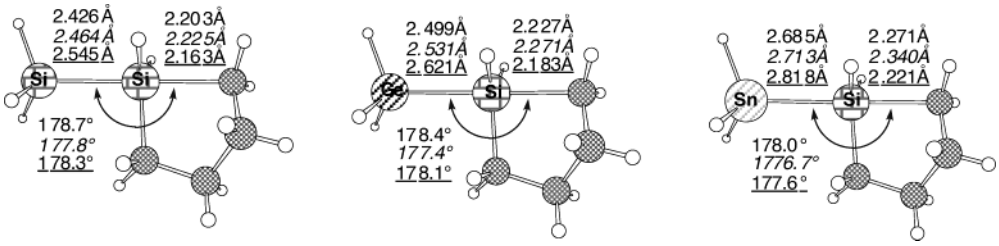

FIGURE 8. MP2/DZP-optimized structure of typical transition state **26** for the *backside* attack mechanism of rring-closure reactions of radicals **9**. B3LYP/DZP in italics. UHF/DZP values are underlined.

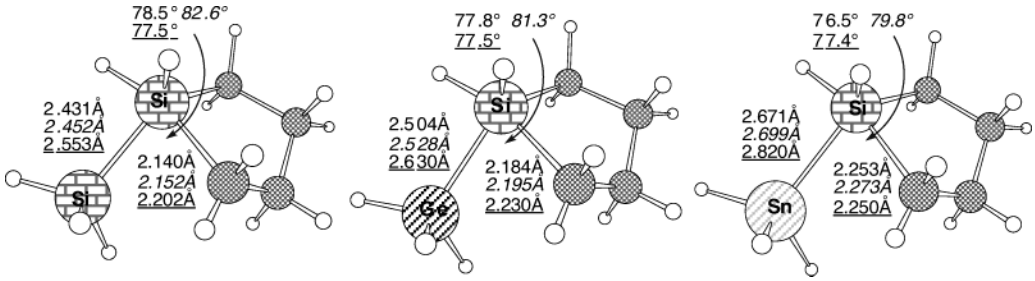

FIGURE 9. MP2/DZP-optimized structure of typical transition state **27** for the *frontside* attack mechanism of ring-closure reactions of radicals **9**. B3LYP/DZP values are in italics. UHF/DZP values are underlined.

SCHEME 11

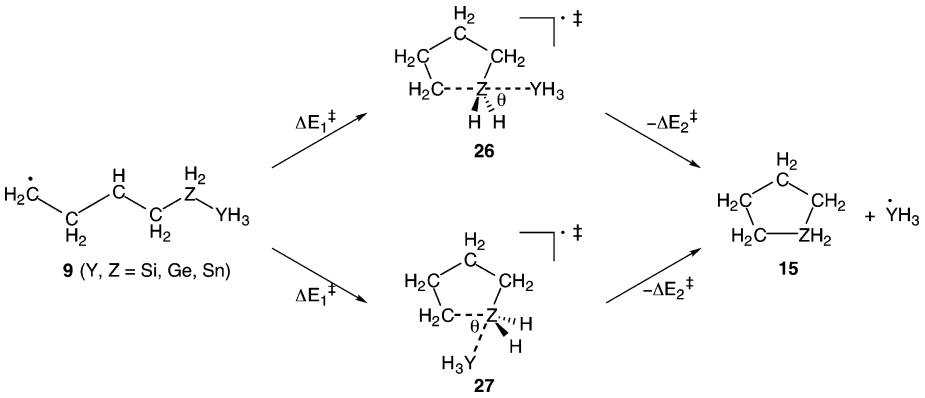

It is interesting to note that four-membered-ring formation reactions prefer the *frontside* attack mechanism at all levels of theory employed. In addition, the energy barriers ($\Delta E_1^{\ddagger}$) for these four-membered ring-closure reactions are calculated to be considerably larger (some 30 kJ/mol at the B3LYP/DZP level) than those for the 1,4-translocation reactions. Clearly then, these cyclization reactions are less favorable than the competing translocation chemistry. In good agreement with available experimental data, no silacyclobutane derivatives were obtained in the chemistry involving the similar 3-[(trimethylstannyl)diphenylsilyl]propyl radical (Scheme 3).[15]

Competitive Ring-Closure Reactions: Formation of Five-Membered Rings. Extensive search of the $H_2CCH_2CH_2CH_2YH_2ZH_3$ (Y, Z = Si, Ge, Sn) potential energy surfaces at the usual levels of theory located structures **26** and **27** as transition states for the formation of the metallacyclopentanes (**15**) with the expulsion of a group IV heteroatom radical (Scheme 11).[24]

Once again, force−constant analysis confirmed that structures **26** and **27** correspond to the *backside* and *frontside* ring-closure transition states, respectively, and that hypervalent intermediates were unable to be located. It should also be noted that no transition state **26** (Z = Sn) could be located at any level of theory employed in this study when the leaving radical was silyl or germyl.

The important geometrical features of typical transition states **26** and **27** are summarized in Figures 8 and 9, respectively, while B3LYP/DZP-calculated energy barriers ($\Delta E_1^{\ddagger}$ and $\Delta E_2^{\ddagger}$, Scheme 6) and corresponding imaginary frequencies are listed in Table 7.

Figures 8 and S8 (Supporting Information) reveals that the *backside* attack structures **26** are able to adopt near collinear arrangements (θ = 168−179°) of the attacking and the leaving species. In addition, the *frontside* structures **27** are predicted to involve attack angles (θ) of about 73−83°, very similar to those involved in the intermolecular chemistry. Analysis of C−Z and Y−Z separations in transition state **26** and **27** reveals that the C−Z distances are shorter and the Y−Z separations

(24) For experimental results on this type of reaction, see: Kulicke, K. J.; Chatgilialoglu, C.; Kopping, B.; Giese, B. *Helv. Chim. Acta* **1992**, *75*, 935. Miura, K.; Oshima, K.; Utimoto, K. *Bull. Chem. Soc. Jpn.* **1993**, *66*, 2348. Studer, A. *Angew. Chem., Int. Ed.* **1998**, *37*, 462. Studer, A.; Steen, H. *Chem. Eur. J.* **1999**, *5*, 759.

TABLE 7. B3LYP/DZP-Calculated Energy Barriers[a] ($\Delta E_1^{\ddagger}$ and $\Delta E_2^{\ddagger}$; Scheme 6) for the Five-Membered Ring-Closure Reactions of Radicals 9 and the Corresponding Imaginary Frequency[b] (ν) of Transition State 26 and 27

		26					27				
Y	Z	$\Delta E_1^{\ddagger}$	$\Delta E_1^{\ddagger}$ + ZPE	$\Delta E_2^{\ddagger}$	$\Delta E_2^{\ddagger}$ + ZPE	ν	$\Delta E_1^{\ddagger}$	$\Delta E_1^{\ddagger}$ + ZPE	$\Delta E_2^{\ddagger}$	$\Delta E_2^{\ddagger}$ + ZPE	ν
Si	Si	55.0	57.7	65.5	66.3	430.9i	64.5	68.6	75.0	77.2	232.9i
Si	Ge	56.5	58.9	52.2	53.3	340.0i	65.8	69.4	61.5	63.8	224.8i
Si	Sn	c					42.6	45.9	25.8	28.0	151.4i
Ge	Si	47.6	49.8	77.6	77.3	430.6i	57.6	61.5	87.7	88.9	251.9i
Ge	Ge	48.4	50.8	61.5	61.3	343.7i	58.6	62.4	71.7	72.9	224.2i
Ge	Sn	c					37.2	41.2	33.8	35.2	155.1i
Sn	Si	40.8	43.1	98.3	96.5	425.2i	47.7	52.1	105.3	105.4	271.8i
Sn	Ge	41.6	44.1	77.6	76.1	346.7i	50.1	53.7	86.1	85.7	226.4i
Sn	Sn	28.1	30.4	42.4	41.4	267.5i	32.0	35.2	46.3	46.1	169.2i

[a] Energies in kJ/mol. [b] Frequencies in cm^{-1}. [c] No transition states were found.

are longer than those in the transition states involved in the analogous intermolecular reactions.[14] In other words, transition states **26** and **27** are "earlier" than the transition state for the intermolecular substitution reactions and also earlier than transition states **24** and **25** for four-memberd ring-formation. The "earliness" of the transition states in question follows the general order five-membered ring-closure > four-membered ring-closure > intermolecular substitution and is also reflected in the energy barriers involved in each case.

Inspection of Table 7 reveals that most of these reactions are predicted to be exothermic, in contrast with the results obtained for the four-membered ring-closure reactions. In addition, and contrary to the results obtained for the four-membered ring-closure reactions, for five-membered ring-formation, both *frontside* and *backside* attack mechanism are predicted to be feasible at all levels of theory. Importantly, the energy barriers ($\Delta E_1^{\ddagger}$) for the five-membered ring-closure reactions are calculated to be similar to those for the intramolecular homolytic substitution reactions and slightly less than those for the 1,5-translocation chemistry that compete with these ring-closure reactions, suggesting that both ring-formation and the translocations are feasible and competitive.

Acknowledgment. The support of the Melbourne Advanced Research Computing Centre is gratefully acknowledged.

Supporting Information Available: Diagrams containing important geometrical features of all transition structures located al all levels of theory employed in this study (Figures S1−S9), calculated energy barriers for all reactions at all levels of theory employed in this study (Tables S1−S7), and Gaussian Archive entries for all optimized structures at all levels of theory employed in this study and higher-level single-point energies. This material is available free of charge via the Internet at http://pubs.acs.org.

JO035037R